Recent advances in the design of quasiaxisymmetric stellarator plasma configurations*

A. Reiman,[1,†,a)] L. Ku,[1] D. Monticello,[1] S. Hirshman,[4] S. Hudson,[1] C. Kessel,[1] E. Lazarus,[4] D. Mikkelsen,[1] M. Zarnstorff,[1] L. A. Berry,[4] A. Boozer,[5] A. Brooks,[1] W. A. Cooper,[2] M. Drevlak,[3] E. Fredrickson,[1] G. Fu,[1] R. Goldston,[1] R. Hatcher,[1] M. Isaev,[7] C. Jun,[1] S. Knowlton,[9] J. Lewandowski,[1] Z. Lin,[1] J. F. Lyon,[4] P. Merkel,[3] M. Mikhailov,[7] W. Miner,[6] H. Mynick,[1] G. Neilson,[1] B. E. Nelson,[4] C. Nührenberg,[3] N. Pomphrey,[1] M. Redi,[1] W. Reiersen,[1] P. Rutherford,[1] R. Sanchez,[8] J. Schmidt,[1] D. Spong,[4] D. Strickler,[4] A. Subbotin,[7] P. Valanju,[6] and R. White[1]
[1]*Princeton Plasma Physics Laboratory, Princeton, New Jersey 08543*
[2]*CRPP-PPB, CH-1015 Lausanne, Switzerland*
[3]*IPP-Euratom Association, D-17491 Greifswald, Germany*
[4]*Oak Ridge National Laboratory, Oak Ridge, Tennessee 37831-8070*
[5]*Department of Applied Physics, Columbia University, New York, New York 10027*
[6]*University of Texas at Austin, Austin, Texas 78712-1081*
[7]*Kurchatov Institute, Moscow, Russia*
[8]*Universidad Carlos III de Madrid, Madrid, Spain*
[9]*Department of Physics, Auburn University, Auburn, Alabama 36849*

(Received 24 October 2000; accepted 28 December 2000)

Strategies for the improvement of quasiaxisymmetric stellarator configurations are explored. Calculations of equilibrium flux surfaces for candidate configurations are also presented. One optimization strategy is found to generate configurations with improved neoclassical confinement, simpler coils with lower current density, and improved flux surface quality relative to previous designs. The flux surface calculations find significant differences in the extent of islands and stochastic regions between candidate configurations. (These calculations do not incorporate the predicted beneficial effects of perturbed bootstrap currents.) A method is demonstrated for removing low order islands from candidate configurations by relatively small modifications of the configuration. One configuration is identified as having particularly desirable properties for a proposed experiment. © *2001 American Institute of Physics.* [DOI: 10.1063/1.1351826]

I. INTRODUCTION

This paper reports on recent advances in quasiaxisymmetric stellarator design that have led to significantly improved predicted performance. The advances have emerged from a continuing design study for the National Compact Stellarator Experiment (NCSX) that has targeted compact stellarator configurations with good transport and stability properties, with quasiaxisymmetry[1,2] used to obtain good drift trajectories. Previous papers have reported on configurations that have emerged from this study.[3–6] The work described in this paper has advanced the study in two major respects: (1) two strategies for further configuration improvement have been explored, leading to an examination of two types of quasiaxisymmetric stellarator configurations whose physics properties we have not previously studied; (2) the requirement of good equilibrium flux surfaces has now been added as a design objective, and the flux surfaces have been evaluated with the PIES three-dimensional equilibrium code.[7]

Throughout this paper, recently generated quasiaxisymmetric (QA) configurations will be compared with an earlier reference QA configuration denoted Configuration C82.[5] The plasma boundary shape of Configuration C82 is shown in Fig. 1, and its ι profile is shown in Fig. 2. The configuration combines many of the desirable features of drift-optimized stellarators with those of advanced tokamaks. As in other drift-optimized stellarators, an underlying symmetry property of the magnetic field is used to provide good drift trajectories. In QA stellarators, the drift trajectories look like those in a tokamak, and the bootstrap current is also comparable to that in a tokamak. The studies of Configuration C82 used a bootstrap-like current profile adopted from the ARIES advanced tokamak studies,[9] and they also adopted the ARIES pressure profile. As in advanced tokamaks, the central region of Configuration C82 has reversed shear, $dq/dr<0$, corresponding to $d\iota/dr>0(\iota=1/q)$. Unlike advanced tokamaks, Configuration C82 takes advantage of the externally generated rotational transform to extend the reversed shear region across the entire cross section. One advantage of $\iota'>0$ is that it is predicted to confer stability to neoclassical tearing modes.[10]

Configuration C82 is calculated to be stable to ballooning modes, external kink modes, and vertical modes at a β of 4%. Ballooning stability is produced by axisymmetric components of shaping, like those used in advanced tokamak designs. The strong axisymmetric shaping is a unique feature

*Paper UI1 1, Bull. Am. Phys. Soc. **45**, 288 (2000).
†Invited speaker.
a)Electronic mail: reiman@pppl.gov

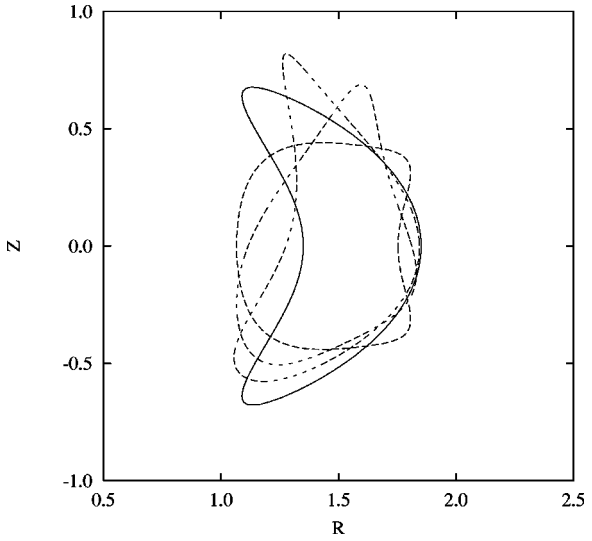

FIG. 1. Plasma boundary shape of Configuration c82 at poloidal cross sections separated 20° toroidally.

relative to other stellarator designs. Unlike advance tokamaks, the external kink mode is passively stabilized in Configuration C82 by a combination of externally generated shear and a stabilizing three-dimensional corrugation of the plasma boundary. (Because of their hollow current profile, advanced tokamaks require a close-fitting conducting wall to stabilize external kink modes, and they require feedback stabilization on the resistive time scale of the conducting wall.) Having stabilized the external kink mode via three-dimensional shaping, we find that the vertical mode is robustly stable, also without need for a conducting wall or feedback stabilization.

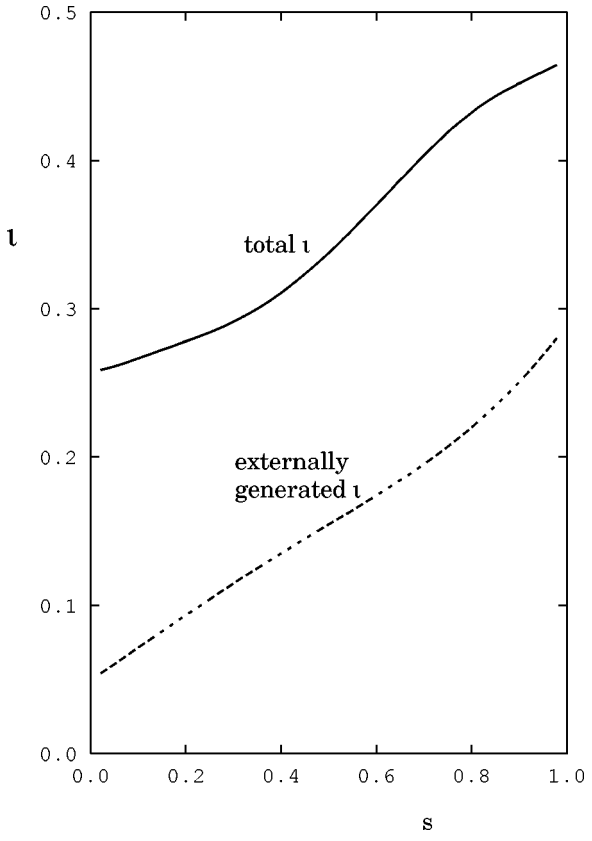

FIG. 2. Rotational transform profile of Configuration c82.

The earlier work on Configuration C82 did not examine the issue of equilibrium flux surfaces. Calculations reported in this paper find substantial flux surface loss in Configuration C82 as β is raised to values of interest. (Although these calculations do not include the effect of perturbed bootstrap currents, which is predicted to decrease island widths[10] for $\iota' > 0$.) As will be discussed in this paper, some of the recently generated configurations are calculated to have good surfaces without relying on neoclassical effects. The equilibrium flux surface calculations described in this paper have been done using the PIES code.[7] For this purpose, a number of modifications have been made to the code to improve its speed, allowing it to be used to routinely evaluate candidate configurations. These modifications are described in Appendix B.

Our previous optimization studies imposed the constraint that candidate configurations fit inside an existing set of toroidal field (TF) coils. [It was desired to reuse the Princeton Beta Experiment (PBX)[8] tokamak TF coils as part of the coil set producing the magnetic field.] This constraint was removed for the study reported in this paper, allowing the exploration of two strategies for further configuration improvement that were previously precluded. This has led us to a study of the physics properties of two types of quasiaxisymmetric configurations that we have not previously examined. One strategy aims at raising the fraction of the rotational transform generated externally and improving vacuum magnetic well properties. An alternative strategy takes advantage of the robust vertical stability produced by our nonaxisymmetric fields to increase the elongation, and thereby raise the stability β limits. The exploration of the different types of configurations was greatly aided by major improvements in the VMEC (Ref. 11) code, which are described in Appendix A, and by the incorporation of a recently developed fast ballooning code COBRA (Ref. 12) in the optimizer.

Section II describes our numerical configuration optimization tools used to evaluate the properties of candidate configurations (other than flux surfaces) and to generate new configurations. Section III discusses the configuration strategies, resulting configurations, and their properties (other than flux surfaces). Recently generated configurations are described that have neoclassical confinement times about 50% longer than that of Configuration C82, and can be generated by simpler sets of nonaxisymmetric coils with lower coil currents. Some of the recently generated configurations have MHD stability β limits as high as 7%, although the existence of flux surfaces at these values of β remains an issue. Section IV discusses equilibrium flux surfaces. Section V contains additional detail on transport properties, flexibility, and startup.

II. CONFIGURATION OPTIMIZATION TOOLS

This section describes the numerical configuration optimization tools used to generate candidate configurations and

TABLE I. Comparison of selected candidate configurations.

	C82	383	2121	3k245b50	3k245b55
No. Periods	3	3	2	3	3
$R/\langle a\rangle$	3.4	4.4	3.16	3	3
β	4.0%	4.1%	4.25%	5.0%[a]	5.5%[a]
Limiting instability	kink	ballooning	both	kink	kink
$\iota(0)$	0.26	0.4	0.20	0.24	0.27
$\iota(a)$	0.47	0.66	0.48	0.48	0.48
$\iota(0)$ vacuum	0.05	0.45	0.25	0.019	0.019
$\iota(a)$ vacuum	0.29	0.49	0.31	0.28	0.27
R (meters)	1.46	1.73	1.4	1.34	1.34
$\langle a\rangle$	0.425	0.397	0.44	0.450	0.400
$w_{\min}$	0.250	0.160	0.166	0.250	0.24
I_p (kA)	200	150	230	277	298
ϵ_h effective	1.0%	0.6%	0.4%	1.4%	1.4%
Ion confinement (ms)	18	28	25	18	18
NBI loss	23%	19%	18%	28%	27%
Coil complexity	3.11	2.05	1.71	2.74	2.79
Max current Density (kA/cm^2)	35.8	17.8	16.5	19.5	21

[a]Stable at $\beta=7\%$ after reoptimization.

to evaluate their properties other than flux surfaces. The calculation of equilibrium flux surfaces is discussed in Sec. IV.

For designing the configurations, the value of β is specified, and an optimizer is used to adjust the values of about 40 parameters specifying the shape of the plasma boundary to attain stability and to target other desired configuration properties. Configuration optimization is performed using a Levenberg–Marquardt scheme to minimize an ''objective function'' which is a sum of squares of desired targets.[13,5] Targets incorporated in the optimizer include: several measures of neoclassical transport [including a confinement time calculated by the DKES (Ref. 14) code and an effective ripple calculated by the Nemov–Kernbichler[15] code]; the eigenvalue of the most unstable external kink; ballooning eigenvalues calculated by the COBRA (Ref. 12) code; the deviation of the rotational transform from prescribed values on one or two flux surfaces; the complexity and current density of an external current sheet constructed by the NESCOIL (Ref. 17) code representing a first approximation to a set of coils. In practice, the configurations obtained in this way represent local optima in configuration space that retain a dependence on the starting point of the optimization calculation. Manual interaction plays a major role in choosing the starting configurations and in adjusting the relative weights of the desired targets. Advances in physics understanding have played a significant role in allowing us to generate configurations with desired properties.

The stability of ballooning, external kink, and vertical modes has been calculated using the Terpsichore (Ref. 16) suite of codes.[20] The CAS3D code has also been used for benchmarking of kink and vertical stability calculations, and to extend kink and vertical stability calculations to the case with the wall at infinity.[21] A recently developed fast ballooning code COBRA (Ref. 12) is also used for ballooning calculations.

Several methods are employed to compare the transport in different configurations. One method uses a measure of the degree of quasiaxisymmetry characterized by an effective ripple strength,[15] calculated numerically to match the $1/\nu$ transport regime. A second method estimates ion thermal confinement times in a deuterium plasma by Monte Carlo simulation using the GTC code to simulate the full ion distribution function.[22] For purposes of the comparison, a model ambipolar potential Φ is used, given by $e\Phi/T_{i0}=s$, where s is the toroidal flux normalized to its value at the plasma boundary. The plasma parameters have been fixed at $T_{i0}=2.14\,\mathrm{keV}$, $n_{e0}=0.67\times10^{14}$, and $B=1.26\,\mathrm{T}$. In addition to the thermal confinement times, we have also calculated the energy losses of 40 keV H-neutral beam ions at $B=2\,\mathrm{T}$ using Monte Carlo simulations.[23,24]

In addition to our physics targets, we have also compared candidate configurations with respect to two quantities that provide a measure of the attractiveness of the associated coils. For this purpose, a set of saddle coils has been constructed for each candidate configuration. As a first step, the NESCOIL code[17] is applied to calculate a sheet current on a coil winding surface external to the plasma that generates the corresponding magnetic field. The sheet current is then discretized into a set of equally spaced coils. The coil winding surface for this calculation is displaced uniformly by 18 cm from the plasma boundary. (The distance of 18 cm was deemed on engineering considerations to be a minimum allowable displacement of the coil winding surface from the plasma for a NCSX scale experiment.) The number of coils in each discretized set is chosen to make the mean error in the normal component of **B** on the plasma boundary approximately equal to 1%.

Two quantities measuring the attractiveness of the coils have been calculated for each candidate configuration. One quantity was calculated directly from the sheet current as $\Sigma\phi_{mn}^2m^2/\Sigma\phi_{mn}^2m$, where the ϕ_{mn} are the Fourier components of the scalar potential for the sheet current, m and n are the poloidal and toroidal mode numbers, and the sum is over all of the Fourier components. This quantity has been found to correlate well with subjective judgment of the complexity

of the associated coils. The quantity is included in Table I for informational purposes, but has not been used as an optimization target in generating the configurations described here. The second quantity calculated is the maximum current density in the discrete coils (for $B=2$ T operation). The coil current density has been identified by engineering analysis as a critical issue due to the thermal stress associated with the temperature rise. For the NCSX saddle coil design, a coil current density limit of about 22 kA/cm^2 has been set as a requirement to establish a threshold below which it is felt that a design solution can be engineered.

In practice, once a configuration selection has been made, several further refinements have been introduced in the engineering design for the corresponding saddle coils, including a more complicated coil winding surface that provides more room for configuration flexibility, and nonuniform spacing of the coils on the winding surface. Although these refinements modify the coil current density somewhat, we have found it convenient and useful to compare relative current densities on the basis of the simplified design procedure described above. In addition, modular coils are also being studied for NCSX. Although the coil comparisons were based on a set of saddle coils, it is found that the existence of attractive modular coil designs also strongly correlates with the values of the two saddle coil measures.

III. CONFIGURATIONS

As outlined in the Introduction, two strategies have been pursued for configuration improvement. The strategies lead us to two types of QA configurations that we have not previously studied. In this section we discuss the optimization strategies, the types of configurations they lead to, and the resulting properties other than flux surfaces. Flux surfaces are addressed in Sec. IV.

Table I compares key properties for selected candidate configurations that will be discussed in this section. Following the stellarator convention, we define the aspect to be $R/\langle a\rangle$. The properties have been evaluated at the values of β indicated. In each case the configuration is marginally stable at that value of β, with the limiting instability indicated. The values of ι at the magnetic axis and the plasma boundary are given for the full current, full β equilibrium, and for the vacuum stellarator field having the same boundary. For the purpose of comparing configurations of different aspect ratio, the major radii have been adjusted to keep the total volume fixed. The quantities $w_{\min}$ and I_p are, respectively, the minimum half-width of the cross section and the total plasma current (evaluated for $B\approx 1$ T).

The earlier reference configuration C82 provides a benchmark against which we compare the new configurations. The neoclassical thermal confinement time in a NCSX scale device based on C82 is estimated to be about 18 ms, which is adequate but marginal for reaching $\beta=4\%$ with the available 6 MW of heating power. The coil current density poses engineering difficulties, and it is considered desirable to reduce this number.

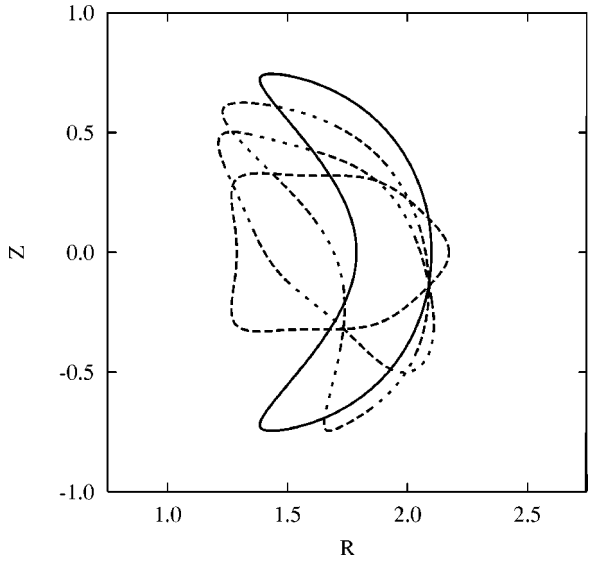

FIG. 3. Plasma boundary shape of Configuration 383 at poloidal cross sections separated 20° toroidally.

A. Increased ι and improved magnetic well

One strategy aims at raising the fraction of the rotational transform generated externally and improving vacuum magnetic well properties. The interest in these goals was initially motivated by a desire to increase the flexibility of the experiment. However, in pursuing these goals, it was discovered that this strategy leads to quasiaxisymmetric configurations of a somewhat different type from C82, and that some of the configurations of this type have improved predicted performance relative to that of C82. A range of configurations of this type has been explored, with aspect ratios from 3 to 5, edge rotational transform from 0.47 to 0.78, rotational transform fraction due to 3D shaping from 50% to 80%, and 2 to 4 periods. A 3-period and 2-period configuration of this type are included in Table I, denoted configurations 383 and 2121. (Although the 2-period configuration has about the same ι as Configuration C82, its transform per period is higher, and the externally generated ι in the core is substantially higher.) Configuration 383 has a neoclassical confinement time about 50% longer than that of Configuration C82, can be generated by simpler sets of nonaxisymmetric coils with lower coil currents, and has improved flux surface quality relative to that of Configuration C82. The plasma boundary shape of configuration 383 is shown in Fig. 3, and its ι profile is shown in Fig. 4.

In practice, configurations of this type have been generated by starting the optimization procedure with a stellarator vacuum field having a moderate magnetic well (typically $\approx 4\%$). Direct targeting of the magnetic well in the full current, full β configuration was not found to be effective, probably because the presence of local optima prevents the gradient following algorithm used in the optimizer from moving to these types of configurations.

An initial motivation for increasing the externally generated ι was the expectation that this would lead to an experiment that would be more flexible in terms of being able to generate a broader range of ι profiles. As we will discuss in

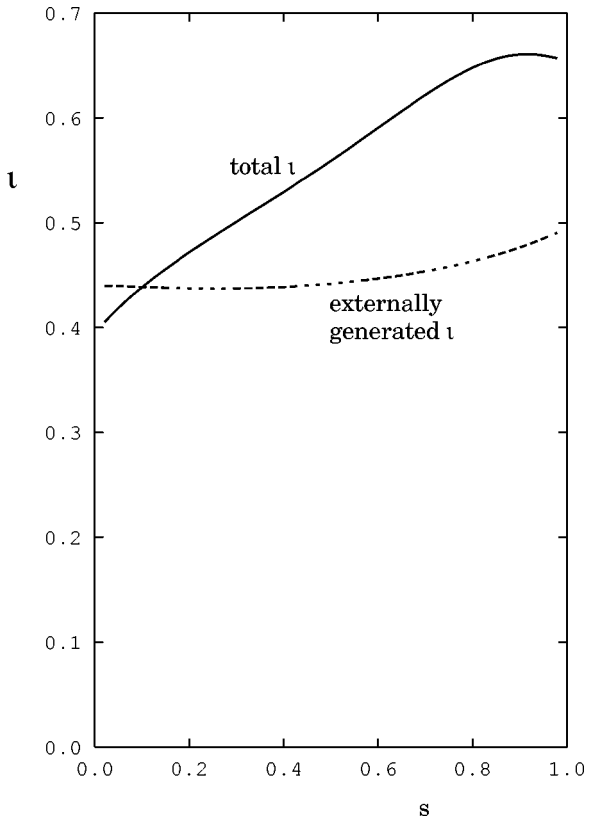

FIG. 4. Rotational transform profile of Configuration 383.

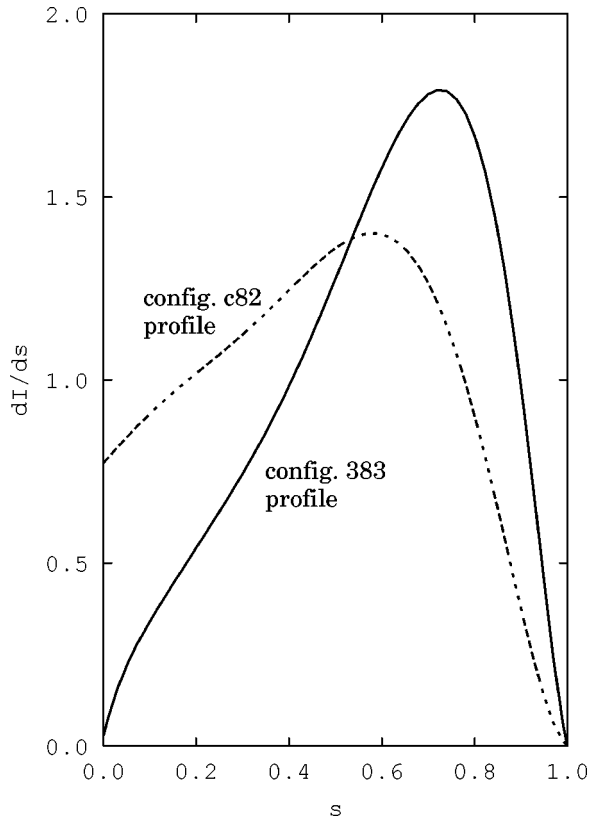

FIG. 5. Current profiles. The normalization is such that $I_p = 1$.

Sec. V, initial flexibility studies indicate that this expectation is borne out. A vacuum magnetic well is also of interest for providing improved flexibility. It allows startup from a vacuum magnetic field with predicted good MHD stability properties at finite β. Configuration C82 does not have a vacuum magnetic well, and MHD stable startup scenarios require some initial driven current before the β is raised.

Comparison of the boundary shapes of Configurations C82 and 383 (Figs. 1 and 3) reveals that the cross-section shapes at $\phi = \pi/3$ are quite different. Configuration C82 has a roughly rectangular cross section at $\phi = \pi/3$. There is an outboard indentation in this cross section that is associated with the three-dimensional corrugation that stabilizes the external kink mode in this configuration. The corresponding cross section in Configuration 383 is pentagonal.

The isosurfaces of local shear have a somewhat different structure in Configuration 383 than in C82.[18] Configuration 383 has helical bands of constant local shear winding entirely around the surface. A helical structure of this type is believed to inhibit the formation of global kink eigenmodes.[19] In Configuration C82, the helical bands are broken in the region near $\phi = \pi/3$, $\theta = 0$.

The increase of $\iota(0)$ eliminates the need for a seed current near the magnetic axis to generate rotational transform there. This has allowed us to adopt a fully self-consistent bootstrap-driven current profile. Figure 5 shows the bootstrap-consistent current profile that we use for configurations of this type, and the current profile with a seed current, used for Configuration C82 and for the elongated configurations described in Sec. III B. The bootstrap-consistent current density goes to zero at the magnetic axis. This increases the shear generated by the plasma current, greatly reducing the shear that must be produced by the externally generated rotational transform. The effect can be seen in the ι values listed for Configurations C82 and 2121 in Table I. While the total shear for Configuration 2121 is somewhat larger than that for C82, the vacuum shear is considerably smaller.

At the same time that we have adopted a bootstrap-consistent current profile for the higher $\iota(0)$ configurations, we have also moved away from the ARIES pressure profile, to one that is more consistent with the stellarator database (Fig. 6).

We have found that as ι is increased at fixed aspect ratio, the nonaxisymmetric ripple tends to increase and Mercier stability tends to deteriorate. The aspect ratio has been modestly increased to compensate for this. For our quasiaxisymmetric configurations, ballooning stability deteriorates with increasing aspect ratio, constraining $R/\langle a \rangle$ from increasing very much. For a device of a given volume, the configurations become increasingly narrow, as measured by $w_{\min}$, as the externally generated ι is increased, increasing penetration of neutrals and placing a practical limit on the externally generated ι. Another constraint on increasing ι is imposed by the increase in coil currents required to produce the larger externally generated transform, and this was found to be the more limiting constraint for a NCSX scale device. (For modular coil designs, the constraint comes in primarily through the increasing difficulty of reproducing the required field at higher ι, rather than through the coil current density.)

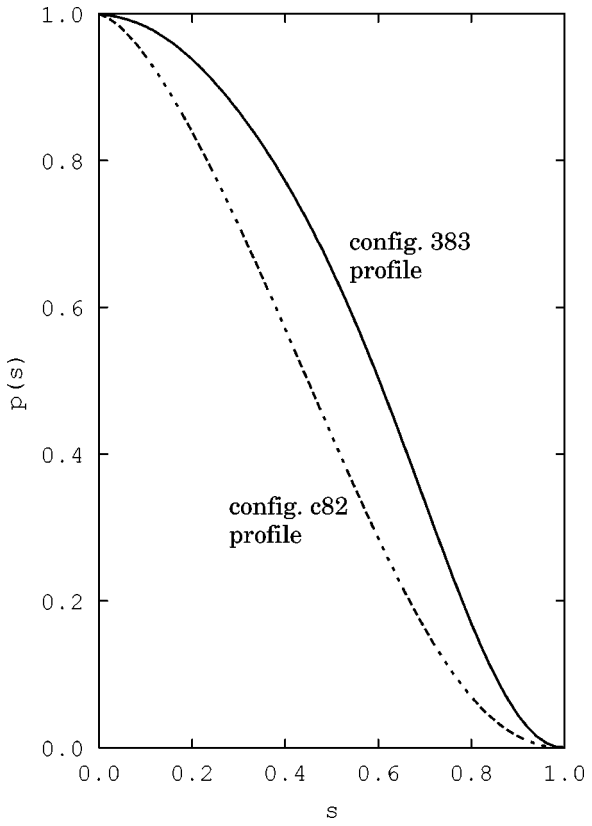

FIG. 6. Pressure profiles. The normalization is such that $p=1$ on axis.

While raising ι we avoid profiles that have low order rational surfaces just inside the plasma boundary. For Configuration 2121, as for C82, $\iota(a)$ is just below 1/2. For Configuration 383, $\iota(a)$ is just below 2/3. We have also found configurations with interesting physics properties having ι entirely above 0.5, with $\iota(a)$ just below 3/4, but these have somewhat higher coil current densities, about 40% higher than that of Configuration 383.

Configurations 383 and 2121 both have improved neoclassical confinement relative to Configuration C82, and substantially reduced coil complexity and coil current density. The magnetic field produced by discrete coils, calculated using the free-boundary VMEC code, does not recover the physics properties of the configuration as well for Configuration 2121 as for Configuration 383. Configuration 383 is deemed more attractive at present as the basis for a physics experiment, but the compactness of the 2-period configurations represented by 2121 makes them a promising subject of further study.

B. Increased axisymmetric elongation

An alternative strategy for configuration improvement takes advantage of the robust vertical stability produced by our nonaxisymmetric fields to introduce stronger axisymmetric components of shaping, and thereby raise the stability β limits. In a tokamak, it follows from Troyon scaling and from the fact that q scales as $(1+\kappa^2)/I_p$, where κ is the elongation and I_p is the total plasma current, that the β limit increases with elongation as $(1+\kappa^2)$. The anomalous confinement scales as I_p, and therefore it, too, improves with increasing elongation at fixed q. The practical limit on elongation in tokamaks is imposed by vertical stability. Elongated tokamaks are unstable to vertical modes in the absence of a stabilizing conducting shell, and require feedback stabilization on the L/R time scale of the conducting shell. Feedback stabilization becomes increasingly difficult as the elongation is increased. Also, at sufficiently high elongation the vertical mode becomes unstable even in the presence of a perfectly conducting wall, depending on the distance of the wall from the plasma.

Although its axisymmetric elongation (1.9) is greater than that in the Aries advanced tokamak design, Configuration C82 is robustly stable to vertical modes even in the absence of a conducting shell, passively stabilized by three-dimensional effects.[25] The robust stability of our configurations to vertical modes allows us to further increase their elongation. Although there is no reason to believe that tokamak-like Troyon scaling is valid for our stellarator configurations, we do expect kink stability to improve with increasing elongation because the fraction of ι generated by the current decreases with increasing elongation. This follows from the fact that the transform generated by a fixed total current scales as $1/(1+\kappa^2)$, while the magnitude of the total bootstrap current in our configurations increases only weakly with increasing κ.

Ballooning stability is also found to improve at higher κ.

A range of elongated configurations of this type was explored with aspect ratios 3 to 5 and elongation values of 2.45, and 3.0. The C82 pressure and current profiles were retained in these studies, with the current constrained in magnitude to be that given by an axisymmetric/collisional formulation of the bootstrap current, and the collisionality set by taking a peak temperature of 2 keV at $\beta=4\%$. Consistent with other studies, the nonquasiaxisymmetric ripple was found to decrease with increasing aspect ratio. A fixed level of non-quasisymmetric ripple was found to be associated with approximately a fixed aspect ratio (fixed $R/\langle a\rangle$) as the elongation was increased. As the elongation is increased at fixed aspect ratio and volume, the cross section becomes increasingly narrow.

Mercier and ballooning modes were found to be stable for all configurations of this type that were studied. The β limits were determined by kink stability. As β is increased in these configurations, kink modes are driven unstable primarily by the increase in magnitude of the bootstrap current. The optimizer can restabilize the kink modes at higher values of β via three-dimensional shaping, at some cost to the nonquasisymmetric ripple (reduced quasiaxisymmetry), to the coil complexity, and to the magnitude of the required coil currents. The fraction of the transform generated by bootstrap current increases at higher aspect ratio, so that kink stability improves at lower aspect ratio.

The parameters of two elongated configurations with differing β limits are listed in Table I. The configurations have the same aspect ratio and elongation. The neoclassical energy confinement time is comparable to that of C82 for $R/\langle a\rangle=3$, and is about 30% higher for $R/\langle a\rangle=4$. The coil complexity and maximum coil current density have been im-

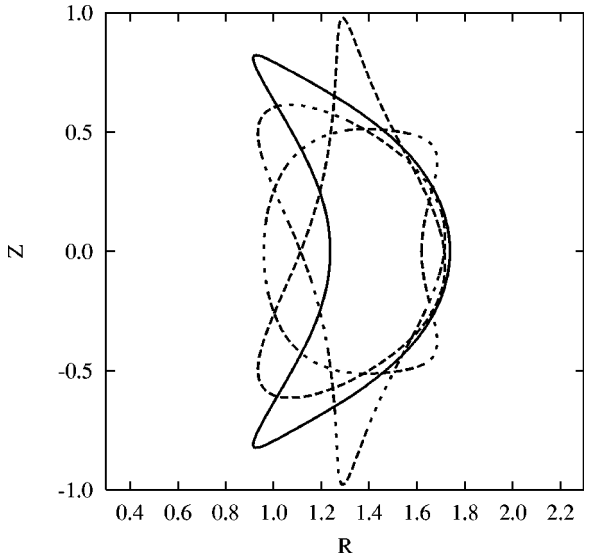

FIG. 7. Plasma boundary shape of Configuration 3k245b50 at poloidal cross sections separated 20° toroidally.

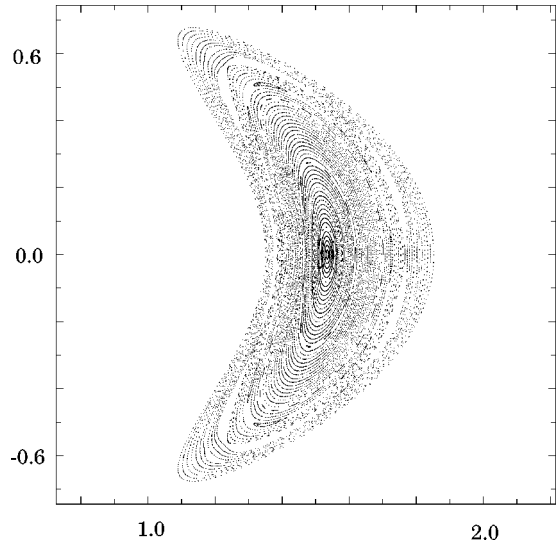

FIG. 8. Poincare plot for Configuration c82 at full current and $\beta=0$.

proved over those of Configuration C82 by targeting these quantities in the optimizer.

Figure 7 shows the plasma boundary of one of the configurations, referred to as 3k245b50. The restabilization of this configuration has been demonstrated for β values as high as 7%. In raising the β limit from 5.0% to 5.5% and then to 7%, the ripple as measured by the largest nonaxisymmetric Fourier component of B in Boozer coordinates increases from 1.88% to 2.07% and then to 2.52%. The increase in ripple in going from $\beta=5.0\%$ to $\beta=5.5\%$ had little impact on the calculated neoclassical transport properties, as can be seen in Table I, where there is little difference in the tabulated properties of the two configurations.

As will be discussed in the following section, Configuration C82 as well as the higher elongation configurations that have been studied have substantial flux surface loss in the absence of neoclassical effects as β is raised to values of interest.

IV. EQUILIBRIUM FLUX SURFACES

Three-dimensional magnetic fields have magnetic islands and regions of stochastic field lines. It is desired to minimize the size of these regions in our configurations to obtain nested flux surface across at least 90% of the cross section. The design procedure that has been adopted for this work specifies the shape of the plasma boundary, and imposes the requirement that it coincide with a flux surface. This places a constraint on flux surface breakup, but is not adequate in itself to guarantee adequate flux surfaces.

Equilibrium flux surfaces have been evaluated using the PIES code.[7] The VMEC code used to calculate three-dimensional equilibria for our stability and transport assessments uses a representation of the magnetic field that assumes nested flux surfaces. The PIES code is a three-dimensional equilibrium code that uses a general representation for the field, and is therefore capable of calculating islands and stochastic field line trajectories. Although the PIES code is capable of doing free-boundary calculations, in which the currents in a set of coils is specified, all of the calculations reported in this paper are fixed boundary calculations, with the shape of the outer flux surface specified. The calculations described in this section were aided by modifications to the PIES code that increased its speed by about an order of magnitude, allowing the routine application of the code to evaluate flux surfaces in candidate configurations. These modifications to the PIES code are described in Appendix B.

In regions where $d\iota/ds>0$, perturbed bootstrap current effects are predicted to lead to substantially decreased magnetic island widths in configurations of the type studied here.[10] This is the inverse of the neoclassical tearing mode that has been observed in tokamak experiments. This neoclassical effect is being incorporated in the PIES code, but has not been included in any of the calculations reported here. The calculations are therefore conservative in that the calculated island widths are likely to be larger than would be observed in an experiment operated in a collisionless regime.

The PIES calculations reported in this section used 143 Fourier modes, $0\leqslant m\leqslant 11$, $-6\leqslant n\leqslant 6$. The calculations for Figs. 8–11 used 60 radial zones, while that for Fig. 12 used 30 radial zones.

Figure 8 shows a Poincare plot of Configuration C82 at full current, $\beta=0$. Magnetic islands occupy about 10% of the cross section. The islands are more readily visible if the Poincare plot uses a polar (ρ,θ) coordinate system, as in Fig. 9. Here, the coordinate ρ is taken to be constant on VMEC flux surfaces, and to measure the distance of the VMEC flux surface from the magnetic axis along the $\theta=0$, $\phi=0$ line. The angular coordinate θ is identical to the VMEC angular coordinate. When plotted in these coordinates, the Poincare plot gives straight lines when the VMEC and PIES solutions coincide.

When β is raised to 3%, the PIES calculations find that a substantial fraction of the flux surfaces are lost (Fig. 10). The equilibrium solution shown is not fully converged. The outer

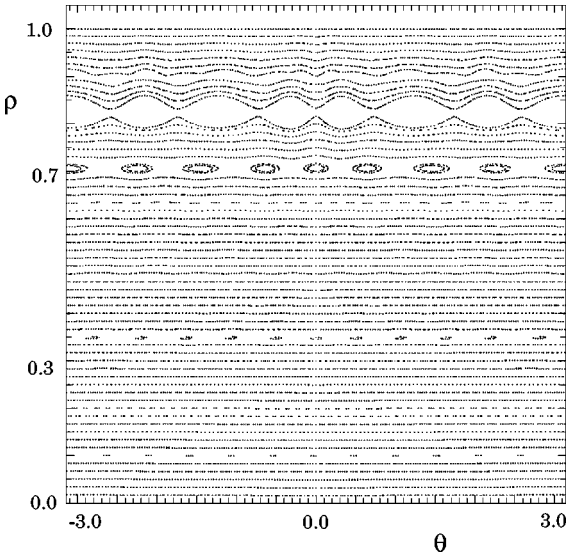

FIG. 9. Poincare plot for Configuration c82 in VMEC coordinates, full current and $\beta=0$.

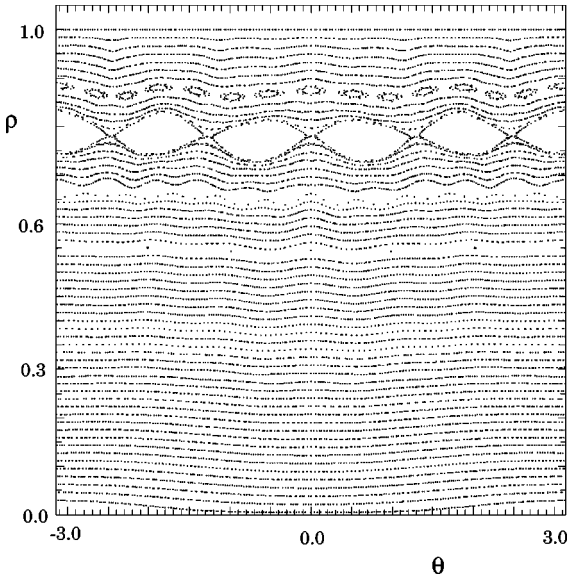

FIG. 11. Poincare plot for Configuration 383 at full current and $\beta=4.2\%$.

surfaces continue to deteriorate as the calculation progresses, so that further computation is of limited interest. Flux surface integrity is a problem for configuration c82 in the absence of stabilizing neoclassical effects.

Figure 11 shows the result of a PIES calculation for Configuration 383 at full current, $\beta=4.2\%$. The flux surfaces are greatly improved relative to those of Configuration c82. The total island width is about 15%, and is dominated by a single island chain at $\iota=0.6$ having poloidal mode number $m=5$ and toroidal mode number $n=3$.

An estimate of the likely magnitude of the improvement from the effect of perturbed bootstrap currents was made for Configuration c82. For this purpose, an analytical calculation was done for narrow islands in cylindrical geometry. To estimate Δ', the high m approximation was used, $\Delta' \approx -2m/r$. To set the collisionality, a central temperature of 2 keV was assumed, and the volume average β was taken to be 3.6%. It was estimated that the $m/n=7/3$ island would be reduced by about a factor of 2 in width.

The fact that the flux surface loss in configuration 383 is dominated by a single island chain suggests that this can be further improved by adjusting the amplitude of the corresponding resonant Fourier mode in the specification of the boundary shape. This has been demonstrated as follows. An algorithm has been implemented which makes small adjustments in the boundary shape to suppress magnetic islands.[26] A series of PIES calculations is used to measure the response of the interior magnetic island widths to modifications in Fourier components specifying the boundary shape. For this purpose, a new diagnostic has been incorporated in PIES for the accurate measurement of small changes in the island

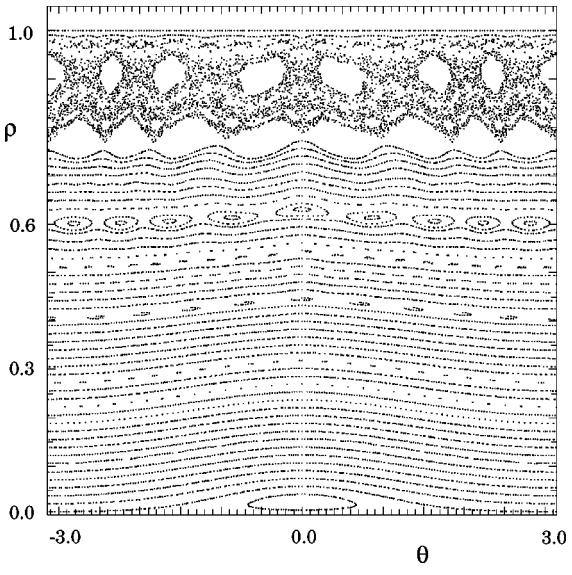

FIG. 10. Poincare plot for Configuration c82 at full current and $\beta=3\%$.

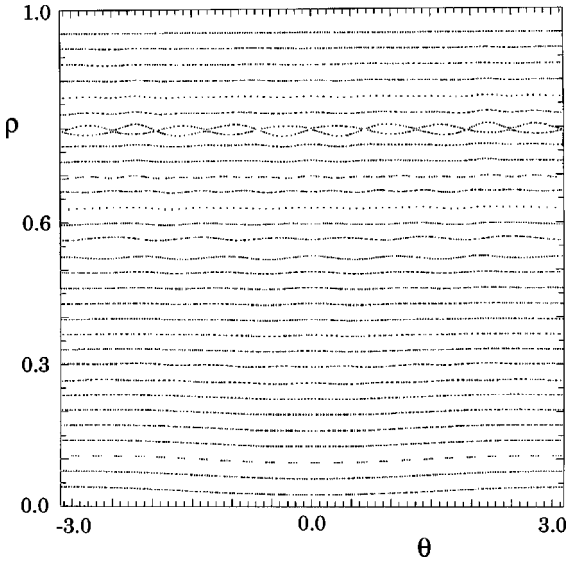

FIG. 12. Poincare plot for modified Configuration 383 at full current and $\beta=4\%$.

widths.[27] A response matrix is constructed, and is used to determine a modified boundary. A PIES calculation evaluates the effect.

This algorithm was applied to Configuration 383. Nine resonant fields in the interior were targeted, $n/m=3/5$, 9/16, 6/11, 9/17, 3/6, 9/19, 6/13, 9/20, and 3/7. The boundary Fourier components adjusted were $n/m=3/4$, 3/5, . . . , 3/8, with the largest Fourier amplitude adjustment about 4 mm. The Poincare plot for the resulting configuration is shown in Fig. 12. The width of the island at the $\iota=0.6$ surface is substantially reduced. The relatively small perturbation of the boundary relative to Configuration 383 is found to have little effect on the stability or quasiaxisymmetry properties of the configuration.

V. FURTHER ASSESSMENT OF TRANSPORT, FLEXIBILITY, AND STARTUP

The work described in this paper has led us to an improved reference configuration, Configuration 383. This section describes further assessments of transport, flexibility and startup issues for Configuration 383.

A. Transport

As described in Sec. II, a model ambipolar potential was used in assessing the relative neoclassical transport of candidate configurations. Self-consistent ambipolar potentials have been incorporated in two methods that have been developed for providing an improved assessment of transport. One method uses a modified version of the GTC code[28] to calculate the ambipolar electric field via a low-noise technique for calculating the particle fluxes from the toroidal variation of $p_{\|}+p_{\perp}$. The second method[29] combines models of the transport processes (helical neoclassical, toroidal neoclassical, anomalous) in a 1D transport solver (STP) to predict temperature profiles and confinement for an assumed density profile. It includes an axisymmetric beam-deposition model and the Monte Carlo code calculated fast-ion losses. Currently, the model for helical neoclassical transport uses the calculated ϵ_{eff} and the Shaing–Houlberg full transport matrix.[30] The models for toroidal neoclassical transport and anomalous transport are from Chang–Hinton[31] and Lackner–Gottardi,[32] respectively. STP calculates the ambipolar electric field, choosing the ion root if it is present. The two methods have been benchmarked and predict the same ambipolar electric field to within 5% and the same ion energy flux within the Monte Carlo simulation uncertainty.

Plasma parameters have been projected by STP for a possible experiment using $R=1.75\,\mathrm{m}$, $B=1\,\mathrm{T}$, and heating power $P=5\,\mathrm{MW}$. The minimum confinement required to achieve $\beta=4\%$ is 1.7 times the ISS-95 scaling prediction at an average density of $1.28\times10^{20}\ \mathrm{m}^{-3}$, the Sudo density limit, resulting in a very collisional plasma. To obtain $\beta=4\%$ at a collisionality $\nu^*=0.25$ at the half-radius requires a density of $4.8\times10^{19}\ \mathrm{m}^{-3}$ and 2.6 times the ISS-95 scaling, comparable to the best achieved on present-day stellarators, but at a very different aspect ratio. The core transport is dominated by the toroidal-neoclassical losses and the calculated helical-neoclassical transport is negligible. Since this configuration is designed to have approximately the same drift orbits as a tokamak and the simulations predict tokamak-like transport, it is reasonable to compare this confinement to tokamak global scalings. If we use an effective equivalent plasma current to evaluate the tokamak scaling, the required confinement to achieve $\beta=4\%$ and $\nu^*=0.25$ is about 1.1 times the ITER-89P prediction. For the same conditions, except $B=2\,\mathrm{T}$, STP predicts central temperatures of 4.8 keV, $\nu^*=0.04$, and $\beta=1.7\%$. This condition should allow access to plasmas with reactor-like collisionality. The core transport is still dominated by the toroidal-neoclassical losses, and the global confinement is equivalent to 0.95 times ITER-89P.

B. Flexibility

The larger fraction of externally generated rotational transform in configuration 383 relative to earlier NCSX designs suggests that variation of the associated coil currents can provide greater flexibility to generate a range of configurations of interest for experimental study. This has been studied by using a free-boundary optimizer to control the coil currents in both saddle coil and modular coil designs for Configuration 383. (An earlier study examined fixed boundary flexibility for Configuration c82.[33]) Both coil designs include a set of poloidal field coils to control plasma position and average shape. The modular coil design has 7 coils per period and includes a weak toroidal solenoid to allow variation of the iota. The saddle coil design has 8 coils per period and uses a toroidal solenoid to generate the toroidal field.

For the flexibility studies, it is assumed that the current in each coil type can be independently controlled (preserving stellarator symmetry). For both types of coil sets, the externally generated ι could be varied across the range from 0.2 to 0.6. The ripple magnitude was constrained to no more than 2.3 times the original optimized configuration, and the plasma was constrained to remain within a design vacuum vessel. A similar study varied the magnetic shear down to approximately shearless at full plasma current. In these cases, the quasisymmetry was degraded by up to a factor of 6.5.

C. Startup

The evolution of the plasma current from vacuum through an Ohmic current-ramp to equilibration with the bootstrap current has been simulated using an assumed temperature evolution. By assuming early auxiliary heating to increase the temperature, as used in reversed-shear tokamak experiments, broad current profiles were predicted which equilibrate with the bootstrap current in 0.5 s. The current evolution was approximated using an axisymmetric calculation, representing the rotational transform from the coils as a constant imposed external current drive profile. The auxiliary heating was assumed to not directly drive parallel current. The calculated current profiles and pressure profiles were used with the free-boundary optimizer to calculate the evolution of coil-currents constraining the plasma shape to stay approximately fixed. Simulation of the evolution from vacuum to $\beta\approx3.2\%$ with a candidate modular coil set showed reasonable coil-current variations and that kink-

modes were calculated to be stable throughout the evolution. In simulations of unidirectional neutral beam injection, the beam driven current strongly changed the core rotational transform. For cotangential only injection, the central rotational transform rapidly goes above one, producing a tokamak-like shear profile which is unstable to neoclassical tearing modes. From these simulations, balanced co- and counterinjection will be required to obtain the optimized current profile. Variations away from balanced injection could provide a means to control the central magnetic shear.

VI. DISCUSSION

This paper has described the results of a series of studies in which two strategies for improving the properties of quasiaxisymmetric (QA) stellarator configurations have been explored. The paper has also described a set of calculations assessing the equilibrium flux surfaces of candidate QA configurations.

One strategy described here for improving QA configurations increases the externally generated ι and also targets improved magnetic well properties. The interest in this was initially motivated by a desire to improve the flexibility of the experiment. It has been found that this approach leads to QA configurations of a type somewhat different from those explored previously, with some of the configurations of this type having improved predicted properties relative to a previous NCSX reference configuration. The difference in the configuration type manifests itself most visibly in a distinct difference of the cross-section shape for the widest cross section. The isosurfaces of constant local shear have a different structure. The increased iota on axis allows the adoption of a fully bootstrap-consistent current profile, with the current density vanishing at the magnetic axis. The increased shear provided by this current profile allows the externally generated rotational transform profile to have much lower shear.

A range of configurations of this type have been studied. Relative to a previous NCSX reference configuration, these configurations have been found to have improved neoclassical confinement, simpler coils with lower current density, and improved flux surface quality. The improvement in physics properties that can be obtained by increasing the externally generated transform in configurations of this type appears to be limited primarily by the increased coil current required at higher externally generated ι. An optimal design will therefore depend on the size and magnetic field of the device to be constructed, and is likely to also be affected by advances in coil engineering. It is also influenced by the margin in coil current density reserved to provide flexibility about the design point. For the NCSX device, the configuration denoted Configuration 383 was judged to be optimal.

The second strategy described for improving QA configurations takes advantage of the robust vertical stability produced by the nonaxisymmetric fields to introduce stronger axisymmetric components of shaping, and thereby raise the stability β limits. By this method, QA configurations with stability β limits as high as 7% have been found. All configurations of this type that have been studied have been found to suffer from substantial flux surface loss in the absence of neoclassical effects.

For a NCSX scale device, we have not found great benefit from combining the two strategies described in this paper, but there may be benefit to doing so in larger devices. It may be possible in this way to increase the stability β limits and simultaneously obtain the advantages obtained at higher externally generated ι and improved magnetic well. A limitation on combining the strategies is imposed by the narrowing of the minimum half-width, denoted $w_{\min}$ in Table I. The value of $w_{\min}$ decreases with increasing externally generated transform, and also with increasing aspect ratio. The value of $w_{\min}$ also decreases at fixed aspect ratio as the elongation is increased. The minimum acceptable value of $w_{\min}$ is set by neutral penetration. For Configuration 383, it was judged that an increase in elongation would make $w_{\min}$ unacceptably small in an $R=1.7$ m device.

The flux surface calculations described in this paper do not include the predicted beneficial effect of perturbed bootstrap currents in the islands, and they impose a fixed boundary at the plasma edge. The earlier reference Configuration C82 is found to lose a substantial fraction of the flux surfaces in the outer region as β is raised to 4%. A similar behavior is found in the configurations produced by increasing the axisymmetric elongation. In contrast, Configuration 383 is found to have much improved flux surfaces. At $\beta=4.2\%$ (Fig. 11) it is calculated to have an island chain at the $\iota=0.6$ surface whose width is about 10% of the minor radius, and to also have other much smaller island chains. The total width occupied by the islands is less than about 15% of the minor radius.

A relatively small modification of the Configuration 383 boundary is found sufficient to substantially reduce the width of the island at the $\iota=0.6$ surface (Fig. 12). This relatively small perturbation of the boundary is found to have little effect on the stability or the quasiaxisymmetry properties of the configuration.

An initial assessment of the flexibility of saddle and modular coils associated with Configuration 383 indicates that they are capable of exploring a range of externally generated ι and shear.

Experimental plasma parameters have been projected for Configuration 383 using a 1D transport solver that includes models for the neoclassical and anomalous transport and calculates the ambipolar electric field. For $R=1.75$ m, $B=1$ T, and a heating power of $P=5$ MW, the minimum confinement required to achieve $\beta=4\%$ is 1.7 times the ISS-95 scaling prediction. To obtain $\beta=4\%$ at a collisionality $\nu^*=0.25$ at the half-radius requires 2.6 times the ISS-95 scaling, comparable to the best achieved on present-day stellarators but at a very different aspect ratio. Using an effective equivalent plasma current to evaluate the tokamak scaling, the required confinement to achieve $\beta=4\%$ and $\nu^*=0.25$ is about 1.1 times the ITER-89P prediction. At $B=2$ T it should be possible to access plasmas with reactor-like collisionality.

The performance of an $R=1.7$ m scale device designed around Configuration 383 is predicted to be sufficient

to study the key physics issues associated with compact, quasiaxisymmetric stellarators, including disruption suppression near the β limit in the presence of substantial bootstrap current, stabilization of ballooning modes in a stellarator via axisymmetric shaping, passive stabilization of external kink modes via 3D shaping, suppression of magnetic islands via neoclassical effects, and anomalous transport scaling, including the possibility of generating transport barriers through external control of the electric field.

ACKNOWLEDGMENTS

We gratefully acknowledge useful discussions with J. Nuehrenberg, C. Hegna, and P. Garabedian.

This research was supported by the U.S. Department of Energy under Contracts Nos. DE-AC-76-CH0-3073 and DE-AC05-00OR22725, by Euratom, and by the Fonds National Suisse de la Recherche Scientifique.

APPENDIX A: IMPROVEMENTS IN THE VMEC CODE

The exploration of a broad range of configurations was greatly aided by major improvements in the VMEC (Ref. 11) code. The VMEC code has been modified to improve the convergence of the inverse equilibrium equations for the Fourier components of R, Z, and λ (the stream function) near the magnetic axis. In previous versions of the code, where lambda is differenced radially on a mesh centered between R, Z nodes, a type of numerical interchange instability has been observed in the neighborhood of the magnetic axis. This has prevented the temporal convergence of 3D solutions with large number of poloidal and toroidal modes (typically, $m<6-8$ was the practical limitation). It has also produced convergence problems at low ι. The new differencing scheme computes the stream function on the same mesh as R and Z (although the output values of λ continue to be on the half-grid for backwards compatibility), which leads to numerical stabilization of the origin interchange. This allows computation of convergent solutions with substantially higher (VMEC) mode numbers ($m<20$), corresponding to much finer spatial resolution and significantly improved force balance in the final equilibrium state. It also allows the calculation of equilibria with lower ι. The output from VMEC is also used to solve the radial force magnetic differential equation for B_s, permitting an accurate assessment for the parallel current, as a function of poloidal mode number, to be performed. Studies of the Hamada condition near low order rational surfaces and comparison with the PIES code are presently underway.

APPENDIX B: IMPROVEMENTS IN THE PIES CODE

The PIES calculations described in this paper were aided by modifications to the code that increased its speed by about an order of magnitude, allowing routine application of the code to evaluate flux surfaces in candidate configurations. The speed of the code was improved by modifications to use an improved method for PIES initialization with a VMEC solution, to convert to a spline representation for field line following, and to store matrix inverses.

The PIES code is considerably slowed relative to VMEC by the more time-consuming algorithm needed to handle a general representation for the magnetic field, and time is saved by initializing PIES using a converged VMEC solution. For this purpose, the under-relaxation scheme in PIES has been modified to provide an improved coupling to VMEC. This involves blending with the VMEC field in the first PIES iteration. The previous under-relaxation scheme blended the currents rather than the fields. The under-relaxation was skipped in the first PIES iteration, allowing a large step from the VMEC field, and slowing ultimate convergence.

The PIES code follows magnetic field lines as a preliminary step to solving the magnetic differential equation determining the Pfirsch–Schlueter current. Conversion from a Fourier representation to a spline representation of the field has speeded up the code by about a factor of 2.

In each iteration of the PIES code, a discretized Ampere's Law is solved by the inversion of a block-tridiagonal matrix. The elements of the blocks are determined by metric elements of a ''background coordinate system'' that does not change from one iteration to the next, allowing time to be saved by storing the inverses of the blocks. For high resolution calculations, this changes the scaling of the code CPU time from m^3n^3k to m^2n^2k, where m and n are the number of poloidal and toroidal modes retained, and k is the number of radial grid surfaces.

[1] J. Nührenberg, W. Lotz, and S. Gori, in *Theory of Fusion Plasmas*, edited by E. Sindoni, F. Troyon, and J. Vaclavik (Soc. Ital. Fisica, Bologna, 1994).
[2] P. R. Garabedian, Phys. Plasmas **3**, 2483 (1996).
[3] A. Reiman, R. Goldston, L. Ku, D. Monticello, H. Mynick, G. Neilson, M. Zarnstorff, I. Zatz, W. Cooper, and A. Boozer, J. Plasma Fusion Res. **1**, 429 (1998).
[4] A. Reiman, L. Ku, D. Monticello *et al.*, in *Proceedings of the 17th IAEA Fusion Energy Conference*, Yokohama, 1998 (International Atomic Energy Agency, Vienna, 1998), paper IAEA-F1-CN-69/ICP/06 (R), Nucl. Fusion Suppl. (to be published).
[5] A. Reiman, G. Fu, S. Hirshman *et al.*, Plasma Phys. Controlled Fusion **41**, B273 (1999).
[6] G. H. Neilson, A. H. Reiman, M. C. Zarnstorff *et al.*, Phys. Plasmas **7**, 1911 (2000).
[7] A. H. Reiman and H. Greenside, Comput. Phys. Commun. **43**, 157 (1986).
[8] N. Sauthoff, N. Asakura, R. Bell *et al.*, in *Plasma Physics and Controlled Nuclear Fusion Research*, Washington, 1990 (International Atomic Energy Agency, Vienna, 1991), Vol. 1, p. 709.
[9] S. C. Jardin, C. E. Kessel, C. G. Bathke, D. A. Ehst, T. K. Mau, F. Najmabadi, and T. W. Petrie, Fusion Eng. Des. **38**, 27 (1997).
[10] C. C. Hegna and J. D. Callen, Phys. Plasmas **1**, 3135 (1994).
[11] S. P Hirshman, W. I. van Rij, and P. Merkel, Comput. Phys. Commun. **43**, 143 (1986).
[12] R. Sanchez, S. P. Hirshman, J. C. Whitson, and A. S. Ware, J. Comput. Phys. **161**, 589 (2000).
[13] D. A. Spong, S. P. Hirshman, J. C. Whitson *et al.*, Phys. Plasmas **5**, 1752 (1998).
[14] W. I. van Rij and S. P. Hirshman, Phys. Fluids B **1**, 563 (1989).
[15] V. V. Nemov, S. V. Kasilov, W. Kernbichler, and M. F. Heyn, Phys. Plasmas **6**, 4622 (1999).
[16] D. V. Anderson, A. Cooper, U. Schwenn, and R. Gruber, ''Linear MHD stability analysis of toroidal 3D equilibria with TERPSICHORE,'' in *Theory of Fusion Plasmas*, edited by J. Vaclavik, F. Troyon, and E. Sindoni (Soc. Ital. Fisica-Editrice Compositori, Bologna, 1988), pp. 93–102.
[17] P. Merkel, Nucl. Fusion **27**, 867 (1987); P. Merkel and M. Drevlak, in *Proceedings of the International Congress of Plasma Physics* and *25th EPS Conference Controlled Fusion and Plasma Physics*, Prague, 1998,

edited by P. Pavlo (European Physics Society, Geneva, 1998), ECA 22C, 1745.
[18]G. Y. Fu, L. P. Ku, M. H. Redi *et al.*, in *Proceedings of the 18th IAEA Fusion Energy Conference*, Sorrento, Italy, 2000 (International Atomic Energy Agency, Vienna, 2000), paper TH3/2.
[19]W. A. Cooper, Phys. Plasmas **7**, 2546 (2000).
[20]G. Y. Fu, L. P. Ku, W. A. Cooper, S. H. Hirshman, D. A. Monticello, M. H. Redi, A. Reiman, R. Sanchez, and D. A. Spong, Phys. Plasmas **7**, 1809 (2000).
[21]C. Nuehrenberg, Phys. Plasmas **3**, 2401 (1996); C. Schwab, Phys. Fluids B **5**, 3195 (1993).
[22]Z. Lin, W. M. Tang, and W. W. Lee, Phys. Plasmas **2**, 2975 (1995).
[23]D. A. Spong, S. P. Hirshman, J. C. Whitson *et al.*, in *Proceedings of the 17th IAEA Fusion Energy Conference*, Yokohama, 1998 (International Atomic Energy Agency, Vienna, 1998), paper IAEA-F1-CN-69/ICP/07, Nucl. Fusion Suppl. (to be published).
[24]M. H. Redi, H. E. Mynick, M. Suewattana, R. B. White, and M. C. Zarnstorff, Phys. Plasmas **6**, 3509 (1999).
[25]G. Y. Fu, Phys. Plasmas **7**, 1079 (2000).
[26]S. R. Hudson, D. A. Monticello, and A. H. Reiman, ''Reduction of islands in stellarator designs,'' Phys. Plasmas (submitted).
[27]S. R. Hudson and R. L. Dewar, Phys. Plasmas **6**, 1532 (1999).
[28]J. L. V. Lewandowski, A. H. Boozer, J. Williams, and Z. Lin, ''Gyrokinetic calculations of the neoclassical radial electric field in stellarator plasmas,'' Phys. Plasmas (submitted).
[29]M. C. Zarnstorff, L. A. Berry, A. Boozer *et al.*, in *Proceedings of the 18th IAEA Fusion Energy Conference*, Sorrento, Italy, 2000 (International Atomic Energy Agency, Vienna, 2000).
[30]D. E. Hastings *et al.*, Nucl. Fusion **25**, 445 (1985).
[31]C. S. Chang and F. L. Hinton, Phys. Fluids **29**, 3314 (1986).
[32]K. Lackner and N. A. O. Gottardi, Nucl. Fusion **30**, 767 (1990).
[33]M. H. Redi, A. Diallo, W. A. Cooper, G. Y. Fu, J. L. Johnson, C. Nuehrenberg, N. Pomphrey, A. H. Reiman, R. B. White, and M. C. Zarnstorff, Phys. Plasmas **7**, 2508 (2000).